ARTICLE

# Quantum Dynamics of Li+HF/DF Reaction Investigated by a State-to-State Time-dependent Wave Packet Approach†

Wen-tao Li[a,b], Mao-du Chen[a], Zhi-gang Sun[b*]

*a. School of Physics and Optoelectronic Technology, Dalian University of Technology, Dalian 116024, China*

*b. State Key Laboratory of Molecular Reaction Dynamics and Center for Theoretical Computational Chemistry, Dalian Institute of Chemical Physics, Chinese Academy of Sciences, Dalian 116023, China*

(Dated: Received on July 14, 2015; Accepted on July 26, 2015)

Using the reactant coordinate based time-dependent wave packet method, on the APW potential energy surface, the differential and integral cross sections of the Li+DF/HF($v$=0, $j$=0, 1) reactions were calculated over the collision energy range from the threshold to 0.25 eV. The initial state-specified reaction rate constants of the title reaction were also calculated. The results indicate that, compared with the Li+DF reaction, the product LiF of Li+HF reaction is a little more rotationally excited but essentially similar. The initial rotational excitation from $j$=0 to 1 has little effect on the Li+DF reaction. However, the rotational excitation of DF does result in a little more rotationally excited product LiF. The different cross section of both reactions is forward biased in the studied collision energy range, especially at relatively high collision energy. The resonances in the Li+HF reaction may be identifiable as the oscillations in the product ro-vibrational state-resolved integral cross sections and backward scattering as a function of collusion energy. For the Li+HF reaction, the rate constant is not sensitive to the temperature and almost has no change in the temperature range considered. For the Li+DF reaction, the rate constant increase by a factor of about 10 in the temperature range of 100−300 K. Brief comparison for the total reaction probabilities and integral cross section of the Li+HF reaction has been carried out between ours and the values reported previously. The agreement is good, and the difference should come from the better convergence of our present calculations.

**Key words:** Quantum wavepacket, Integral and differential cross section, Reaction rate constant, Li+HF/DF, Isotope effect

## I. INTRODUCTION

The Li+HF reaction is the lightest member of alkali atom plus hydrogen halide family, which has been extensively studied in crossed molecular beam reactive scattering experiments. The first experiment study for the Li+HF system was performed by Taylor and Datz, using the crossed molecular beams method in 1955 [1]. After then, numerous theoretical and experimental studies have been reported in the next few decades. There are several interesting features of the title reaction that make it a prototype for a study of atom-diatom reaction. First, the Li+HF reaction is a prototype system for experimental studies of the "harpoon" mechanism [2]. Second, LiHF is amenable to *ab initio* calculations beyond chemical accuracy. So, various of potential energy surfaces (PES) for the $X^2A'$ symmetry electronic ground state have been reported in Refs.[3–18]. Third, the Li+HF system comprise light atoms with relatively few electrons, which makes it be easy to implement classical and quantum approach. Especially, the angular distributions [$N(\theta)$] of product molecules and integral reactive cross sections ($\sigma_R$) of LiF formation were first reported in experiment by Becker *et al.* in 1980 [19], which could be compared directly with the experiment data.

In experiment, the crossed molecular beam approach is the main way in the experimental investigations, with which the steric effects [20], the evidence for the deep potential well of Li+HF system [21], the laboratory angular distributions (LAB ADs) [22], the relationship between the cross sections, and the translational energy of the reactants [23], the rotational excitation effect on the Li+HF system [23], the double differential cross sections [24], and the angular and time-of-flight distributions of the product LiF [25] have been investigated. In these experiment reports, the quasi-classical trajectory (QCT) method [22, 25] calculations were frequently em-

†Dedicated to Professor Qing-shi Zhu on the occasion of his 70th birthday.

*Author to whom correspondence should be addressed. E-mail: zsun@dicp.ac.cn

 ©2015 Chinese Physical Society

ployed to understand the experiment data.

Numerous theoretical studied [13, 14, 26–46] have been done for the Li+HF reaction. The calculations of the Li+HF reaction performed by the QCT [22, 25, 26, 28, 36, 39], quantum mechanical with reduced dimensionality approach [27, 29], three-dimensional time dependent wave packet approach [13, 32, 34, 37, 40, 45, 46] and quantum time independent method [30, 31, 38, 41–44] have been reported. In their work, various properties of the title reaction have been studied, such as, total reaction probability, state-to-state reactive probabilities, stereodynamics steric effect [20, 33], quantum stereodynamics for different initial states of the reagent [34, 46], integral cross section (ICS), different cross section (DCS), and the reactants polarization of the Li+HF reaction have been studied. The characteristics of the Li+HF reaction at ultralow temperature [41], quantum isotopic effects [38], and the correlation of attack and recoil angles [43, 44] have also been studied. Although a number of theoretical work have been done, the reaction rate constant and the effect of rotational excitation for the Li+DF reaction, and the isotope effects at the state-to-state level have not been fully investigated. In this work, using the time-dependent wave packet theory we performed the dynamical calculations of the Li+HF/DF reaction.

## II. THEORY

For the A+BC→AB+C/AC+B type reaction, three sets of body-fixed (BF) Jacobi coordinates are used to represent the wave functions for different arrangements. The A+BC reactant channel, AB+C and AC+B product channel denoted as $\alpha$, $\beta$, and $\gamma$, respectively. The coordinates are written as ($R_v$, $r_v$, $\theta_v$, $\mathbf{\Omega}_v$), where $v$ is either $\alpha$, $\beta$ or $\gamma$. For $v$=$\alpha$ ($v$=$\beta$, $\gamma$), $r_v$ is the bond distance of the reactant diatom molecule (BC, AB, AC), $R_v$ is the distance from the reactant atom (A, B, C) to the center of mass of (BC, AB, AC), $\theta_v$ is the angle between $r_v$ and $R_v$, $\mathbf{\Omega}_v$ denotes the Euler angles orienting $\mathbf{R}_v$ in the space fixed (SF) frame. In the reactant coordinates, the Hamiltonian for a given total angular momentum $J$ can be written as

$$\hat{H} = -\frac{\hbar^2}{2\mu_{R_\alpha}}\frac{\partial^2}{\partial R_\alpha^2} - \frac{\hbar^2}{2\mu_{r_\alpha}}\frac{\partial^2}{\partial r_\alpha^2} + \frac{(\hat{J}-\hat{j})^2}{2\mu_{r_\alpha}R_\alpha^2} + \frac{\hat{j}^2}{2\mu_{r_\alpha}r_\alpha^2} + V \quad (1)$$

where $\hat{J}$ is the total angular momentum operator, and $\hat{j}$ is the rotational angular momentum operator of BC. The wave function in the BF frame can be expressed as

$$\Psi^{JM\epsilon}(\mathbf{R}_\alpha, \mathbf{r}_\alpha) = \sum_{K_\alpha} \bar{D}^{J^*\epsilon}_{MK_\alpha}(\mathbf{\Omega}_\alpha)\psi_\alpha(R_\alpha, r_\alpha, \theta_\alpha^{K_\alpha}; K_\alpha) \quad (2)$$

where $\bar{D}^{J\epsilon*}_{MK_\alpha}(\mathbf{\Omega}_\alpha)$ is the parity-adapted normalized rotation matrix. Depending only on the Euler angles $\mathbf{\Omega}_\alpha$,

$$\bar{D}^{J\epsilon^*}_{MK_\alpha}(\mathbf{\Omega}_\alpha) = \sqrt{\frac{2J+1}{8\pi(1+\delta_{K_\alpha 0})}}[D^{J^*}_{MK_\alpha}(\mathbf{\Omega}_\alpha) + \epsilon(-1)^{J+K_\alpha}D^{J^*}_{M-K_\alpha}(\mathbf{\Omega}_\alpha)] \quad (3)$$

where $\epsilon$=$(-1)^{j+l}$ is the parity of the system, $l$ is the orbital angular momentum quantum number, $K_\alpha$ is the projection of the total angular momentum $J$ on the BF $z$ axis, and $D^{J\epsilon^*}_{MK_\alpha}(\mathbf{\Omega}_\alpha)$ is the Wigner rotation matrix. The wave function $\psi_\alpha(R_\alpha, r_\alpha, \theta_\alpha^{K_\alpha}; K_\alpha)$ only depending on the internal coordinates $(R_\alpha, r_\alpha, \theta_\alpha^{K_\alpha})$ and $K_\alpha$, can be expanded as

$$\psi_\alpha(R_\alpha, r_\alpha, \theta_\alpha^{K_\alpha}; K_\alpha) = \sum_{n,m,j}[F^{K_\alpha}_{nmj}u_n(R_\alpha)\cdot \phi_m(r_\alpha)Y_{jK_\alpha}(\theta_\alpha) \quad (4)$$

where $n$ and $m$ are the radial basis labels, and $Y_{jK_\alpha}$ are spherical harmonics. The initial wave packet $\Psi^{JM\epsilon}_{v_0j_0l_0}$ is constructed as the product of a total angular momentum eigenfunction, a rovibrational eigenfunction of molecule BC and a Gaussian wave packet in the SF frame. To propagate the initial wave packet in the BF frame, we need transform it from SF frame to BF frame and then propagate it using the forth order split operator method [51]. During the propagation, the fast Fourier-Sine transform method is adopted to act the radical kinetic energy operator onto the wave packet on a $L$-shaped grid. The generalized discrete variable representation (DVR) is used to evaluate the action of the potential energy operator, in which the wave packet is converted from the angular finite basis representation (FBR) to a grid representation. To avoid the wave packet reflecting back from the boundaries, absorbing potentials are employed with the same form as in Ref.[47].

To extract the state-to-state S-matrix for both product channels, the coordinate transformation RCB method is adopted. Because $R'_v$ is fixed at the projection plane $R'_{v0}$, the product wave function has only two degrees of freedom, $r_v$ and $\theta_v$ in the coordinate transformation approach. Then, an "intermediate" coordinate system is employed to implement the RCB method, in which $R_v$ is combined with either ($R_\alpha$, $\theta_\alpha$) or ($r_\alpha$, $\theta_\alpha$), is chosen to provide a convenient platform for projection.

The two-dimensional product internal eigenfunctions are transformed and stored in the reactant grid before propagation. In each propagation step, the wave packet is transformed to the same grid by two one-dimensional transformations, facilitating the calculation of the overlaps. The computational costs are equivalent to those required for evaluating a norm. Finally, the BF frame needs to be rotated into the corresponding new reference axis.

The BF time-independent scattering wave function

DOI:10.1063/1674-0068/28/cjcp1507151 ©2015 Chinese Physical Society

from an initial state ($v_0$, $j_0$, $l_0$) is obtained by an orthogonal transformation matrix as

$$\Phi^{J\epsilon}_{v_v j_v l_v \leftarrow v_0 j_0 l_0}(E) = \sum_{K_v} C^{J j_v \epsilon}_{l_v K_v} \Phi^{J\epsilon}_{v_v j_v K_v \leftarrow v_0 j_0 l_0}(E) \quad (5)$$

The state-to-state scattering matrix $S^{J\epsilon}_{v_v j_v l_v \leftarrow v_0 j_0 l_0}(E)$ ($v$=$\beta$, $\gamma$) in the SF frame can then be obtained by imposing the asymptotic boundary conditions,

$$\Phi^{J\epsilon}_{v_v j_v l_v \leftarrow v_0 j_0 l_0}(E; R_{v0}) = -A(E) \left( \frac{2\pi\hbar^2 k_{v_v j_v}}{\mu_{R_v}} \right)^{1/2} \cdot S^{J\epsilon}_{v_v j_v l_v \leftarrow v_0 j_0 l_0}(E) \bar{H}_{l_v}(k_{v_v j_v} R_{v_0}) \quad (6)$$

where $A(E)$ is defined as

$$A(E) = \left( \frac{\mu_{R_\alpha}}{2\pi\hbar^2 k_{v_0 j_0}} \right)^{1/2} \int \bar{H}_{l_0}(k_{v_0 j_0} R_\alpha) G(R_\alpha) \mathrm{d}R_\alpha \quad (7)$$

where $\bar{H}$ is an outgoing Riccati-Hankel function.

Finally, the scattering matrix $S^{J\epsilon}_{v_v j_v l_v \leftarrow v_0 j_0 l_0}(E)$ in the SF frame is transformed into the helicity representation by the standard transformation.

$$S^J_{v' j' K' \leftarrow v j K} = \sum_{l' l} i^{l-l'} \sqrt{\frac{2l'+1}{2J+1}} \langle j' K' l' 0 | J K' \rangle \cdot S^J_{v' j' l' \leftarrow v j l} \sqrt{\frac{2l+1}{2J+1}} \langle j K l\ 0 | J K \rangle \quad (8)$$

By substituting the scattering matrix $S^{J\epsilon}_{v_v j_v l_v \leftarrow v_0 j_0 l_0}(E)$ in the helicity representation into the standard formulas, we obtain the state-to-state integral cross sections,

$$\sigma_{v_v j_v \leftarrow v_0 j_0} = \frac{\pi}{(2j_0+1)k^2_{v_0 j_0}} \cdot \sum_{K_v} \sum_{K_0} \sum_{J} (2J+1) \left| S^J_{v_v j_v K_v \leftarrow v_0 j_0 K_0} \right|^2 \quad (9)$$

And the state-to-state differential cross sections,

$$\frac{\mathrm{d}\sigma_{v_v j_v \leftarrow v_0 j_0}(\vartheta, E)}{\mathrm{d}\Omega} = \frac{1}{2j_0+1} \sum_{K_v} \sum_{K_0} \left| \frac{1}{2ik^2_{v_0 j_0}} \cdot \sum_J (2J+1) \mathrm{d}^J_{K_v K_0}(\vartheta) S^J_{v_v j_v K_v \leftarrow v_0 j_0 K_0} \right|^2 \quad (10)$$

In which $\vartheta$ is the scattering angle between the incoming A+BC reactants and the scattered AC+B/AB+C products. The initial state-specific reaction rate constant is calculated by thermally averaging the translational energy of the corresponding cross section as

$$k_{v_0 j_0}(T) = \left( \frac{8kT}{\pi\mu} \right)^{1/2} (k_\mathrm{B}T)^{-2} \cdot \int_0^\infty E \mathrm{e}^{-E/k_\mathrm{B}T} \sigma_{v_0 j_0}(E) \mathrm{d}E \quad (11)$$

where $E$ is the translational energy, $k_\mathrm{B}$ is the Boltzmann's constant. Finally, the thermal rate constant can be calculated from the Boltzmann averaging of the initial state specific reaction rate constants as

$$k(T) = \frac{\sum_{v_0 j_0} (2j+1) k_{v_0 j_0}(T) \mathrm{e}^{-E_{v_0 j_0}/k_\mathrm{B}T}}{\sum_{v_0 j_0} (2j+1) \mathrm{e}^{-E_{v_0 j_0}/k_\mathrm{B}T}} \quad (12)$$

where $E_{v_0 j_0}$ is the rovibrational energy of the diatom molecule.

In this work, we will restrict our study to reactions with the reagent HF in its ground rovibrational state, *i.e.* $v_0$=$j_0$=0. For the reagent DF, the initial rovibrational state is $v_0$=$j_0$=0 and $v_0$=0, $j_0$=1, respectively.

## III. RESULT AND DISCUSSION

The numerical parameters used in the calculations on the $L$-shaped grid include: (i) grid range and size: for $R$∈(1.0,20.0), $N^\mathrm{tot}_R$=159 and $N^\mathrm{int}_R$=39, for $r$∈(1.0,25.0), $N^\mathrm{tot}_R$=191 and $N^\mathrm{int}_R$=23; (ii) angular basis $j$=[0, 70]; (iii) Initial wave packet: $R_0$=14.0, $\delta$=0.25, $E_0$=0.2 eV; (iv) matching plane $R'_{v0}$=20.0; (v) absorbing potential: $C^R_1$=0.002, $C^R_2$=0.05,$C^r_1$=0.01,$C^r_2$=0.08, $n$=$n'$=2, $R_a$=15.0, $R_b$=19.0, $r_a$=21.4, and $r_b$=23.7; (vi) total propagation time: 2500 iterations with $\Delta_t$=80.0. Wave packet calculations $\varphi_{k_0}(R)$ have been performed for the Li+HF/DF system with the total angular momentum $J$ up to 43. Intial wave packet is calculated as follows,

$$\varphi_{k_0}(R) = \left( \frac{1}{\pi\delta^2} \right)^{1/4} \mathrm{e}^{-(R-R_0)^2/2\delta^2} \mathrm{e}^{-ik_0 R} \quad (13)$$

The APW PES by Aguado *et al.* [18] has been adopted in this work. As shown in Fig.1, there is a well in the entrance channel with depth about −0.25 eV, corresponding to the Li-HF complex. There is also a shallow well about 0.07 eV in the product channel, corresponding to the LiF-H complex. The saddle point of electronic ground state comes from the crossing between ionic state ($Li^+$+$HF^-$) and a covalent ($Li(^2S)$+$HF(X^1\Sigma^+)$) electronic state. The features of this PES have been discussed in detail by González-Sánchez *et al.* [46] and are very similar to those reported previously [14, 34].

### A. Reaction probabilities

The total reaction probabilities of several selected angular momentum $J$=0, 10, 20, 30, 40, and 44 are collected in Fig.2 as a function of collision energy. As shown in Fig.2 the threshold increases with increasing value of $J$, due to the increasing centrifugal barrier $J(J+1)/2\mu_R R^2$. It is observed that, with the $S$-matrix

DOI:10.1063/1674-0068/28/cjcp1507151 ©2015 Chinese Physical Society

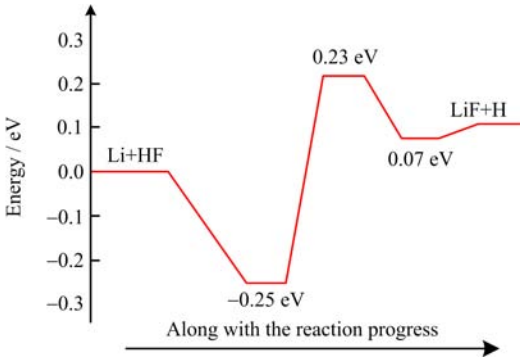


FIG. 1 The minimum energy path along with the reaction progress [18].

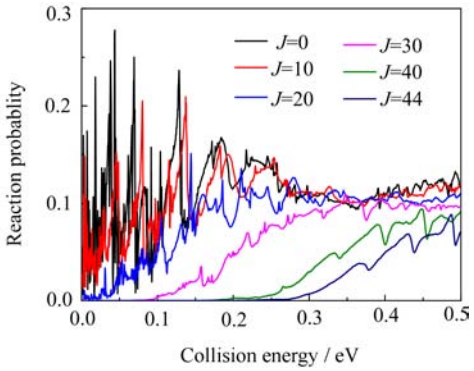


FIG. 2 Total reaction probability of the Li+HF($v$=0, $j$=0) reaction of several selected angular momentum $J$ values, as a function of collision energy.

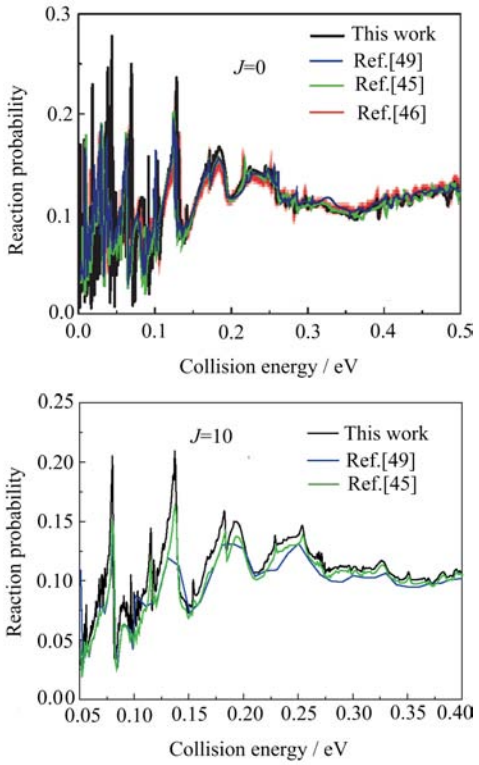


FIG. 3 Total reaction probabilities of the Li+HF($v$=0, $j$=0) with total angular momentum $J$=0 and 10, along with those reported in previous work. The black line are the results of present work, and the blue, green, and red lines are obtained results in Refs.[45, 46, 49], respectively. The agreement is good, however, difference does exist. Our present results are more accurate.

up to $J$=44, the ICS and DCS converge up to about 0.25 eV.

Since there are quite several similar studies on this reaction, in Fig.3, our calculated total reaction probabilities for the Li+HF reaction with the total angular momentum $J$=0 and 10 are shown for a collision energy range of 0−0.5 eV, along with results [45, 46, 49].

From the results in Fig.2 and Fig.3, the reaction probability with $J$=0 exhibits many sharp peaks in the low collision energy region from 0 eV to 0.15 eV, which comes from the long-lived resonance states above the van der Waals well in the reactant channel. In this collision energy range, as shown in Fig.3, there are some differences between the total reaction probabilities, obtained in Refs.[45, 46, 49] and in our present work. The ABC code is employed in Ref.[49] with limited basis set, and the maximal helicity quantum number $K_{\max}$ employed in Ref.[49] was truncated, unlike in our work all of the allowed $K$ have been included. In our present work a fourth-order split operator method is employed and a total propagation time 200000 atomic unit [51, 52] whereas the approach [46] is a real Chebyshev integrator with total iteration number of 20000 for $J$<35. It can be estimated that a longer total propagation time is applied in our work [48]. At the same time, one may notice that the angular basis used [46] is only 50 but with $r_{\max}$=17.5 Å≈33.1 a.u., which is smaller than the basis set ($j_{\max}$=71) used in our work. However, we actually used a smaller $r_{\max}$=25.0 a.u. which is large just right to extract a converged state-to-state $S$-matrix. It is possible that the angular basis set applied in the work [45, 46] cannot give fully converged results. Therefore, it is not surprising that there is some difference between Refs.[45, 49] and our present work, and we do think that our present results are of higher accuracy.

### B. Integral cross sections and differential cross sections

The ICS of the Li+HF($v$=0, $j$=0) reaction is plotted in Fig.4 for collision energy range of 0−0.25 eV, compared with the theoretical and experimental results reported in Refs.[23, 45, 49, 50]. The green and red curves (Ref.[49]) were calculated using the PES [17] and APW PES [18], respectively. As shown in Fig.4, the amplitude of the ICS calculated in our present work decreasse sharply around the threshold energy and exhibits fast oscillations in collision energies range from 0 eV to 0.15 eV. Apparently, these narrow structures

DOI:10.1063/1674-0068/28/cjcp1507151 ©2015 Chinese Physical Society

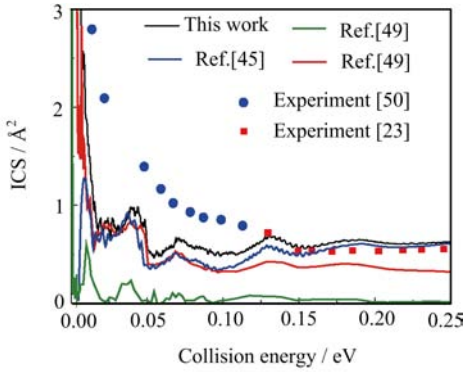


FIG. 4 Comparison of the total integral cross section of the Li+HF($v$=0, $j$=0) reaction obtained in the present work, and the experimental and theoretical ICSs reported in the literatures.

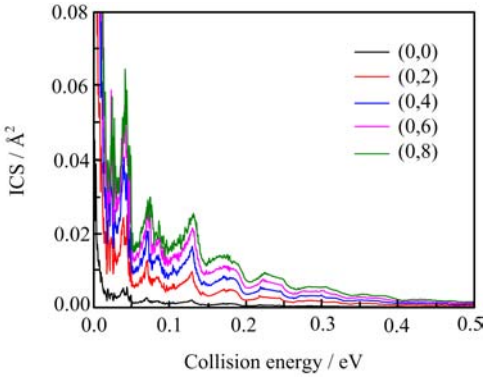


FIG. 5 Product rotational state-resolved integral cross sections of the Li+HF($v$=0, $j$=0)→LiF($v$=0, $j$=0−8)+H reaction.

are attributed to the resonances supported by the potential well in the entrance valley. With collision energy above 0.15 eV, the ICS oscillates in a much milder way. The results obtained [45] agree well with our results at the relative high collision energy. However, significant difference is observed in the lower collision energy part, which may be due to the limited total propagation time and basis set for the angular degree of the freedom. The calculated results given in Ref.[49] agree with our results well, and their difference increases with increasing collision energy. Our ICS agrees with the experimental data [23, 50] in a reasonable way, but unable to give the sharp decrease with increasing collision energy from 0.05 eV to 0.25 eV.

The difference between theoretical and experimental ICS may be due to the following two reasons. First, the ICS at low collision energy part depends strongly on the details of the barrier height and long range interaction potential of the PES, which may be not accurate enough. Second, compared with the experimental ICS, the ICS contributed by rotational excited states need to be thermally included, however, in our present work only initial state with $j_0$=0 was considered. We will investigate this issue in our future work.

The product rotational state-resolved ICS as a function of collision energy for the Li+HF reaction are presented in Fig.5 for the ground vibrational state ($v$=0). It is interesting to see that for different rotational states, the ICSs have peaks at similar collision energies, and decrease with increasing collision energy in a similar amplitude.

The product ro-vibrational state distributions for the Li+HF reaction at four selected energies are shown in Fig.6. At collision energy of 0.0218 eV, there is product only with ground vibrational state. With increasing collision, product with vibrational excited state arises. The rotational state distribution is quite hot, especially at the collision energy of 0.2410 eV.

The reaction with low collision energy mainly happens through tunneling effect via long-lived resonance

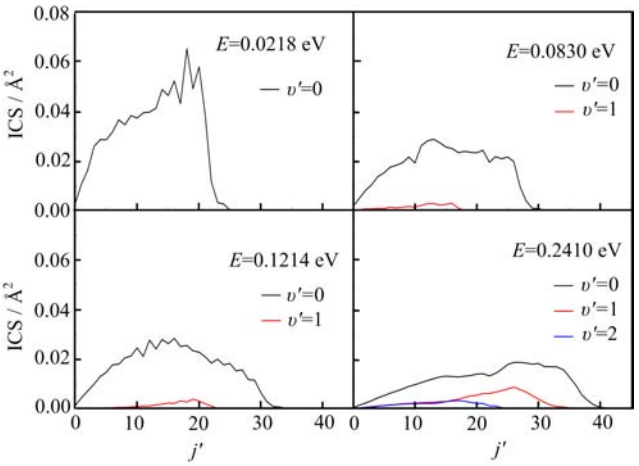


FIG. 6 The rotational state distribution of the product for the Li+HF reaction at collision energies of 0.0218, 0.0830, 0.1214, and 0.2410 eV.

state. As a result, forward and backward scattering is almost symmetric at 0.0850 eV. However, with increasing collision energy, the scattering becomes more and more forward-baised, shown in Fig.7.

The theoretical DCSs of the Li+HF reaction were compared with the experimental results reported in Ref.[24] at collision energy of 0.0882 and 0.1710 eV in Fig.8. The agreement is good, especially at the collision energy of 0.0882 eV, where both theoretical and experimental results are symmetric in forward and backward scattering. Whereas, for the higher collision energy of 0.171 eV, our theoretical results have apparently more forward scattering. The disagreement between experimental and theoretical results may be due to the more importance of the initial rotationally excited states at higher collision energy, which are not included in our present work.

DOI:10.1063/1674-0068/28/cjcp1507151 ©2015 Chinese Physical Society

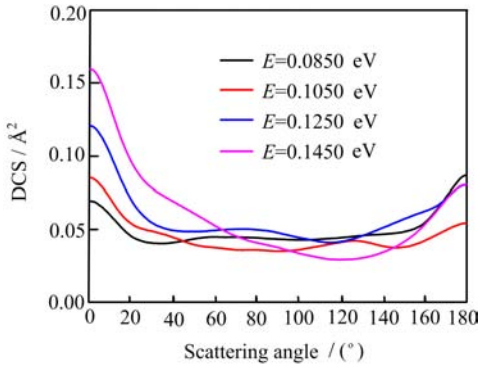


FIG. 7 The differential cross section of the Li+HF reaction for some selected collision energy.

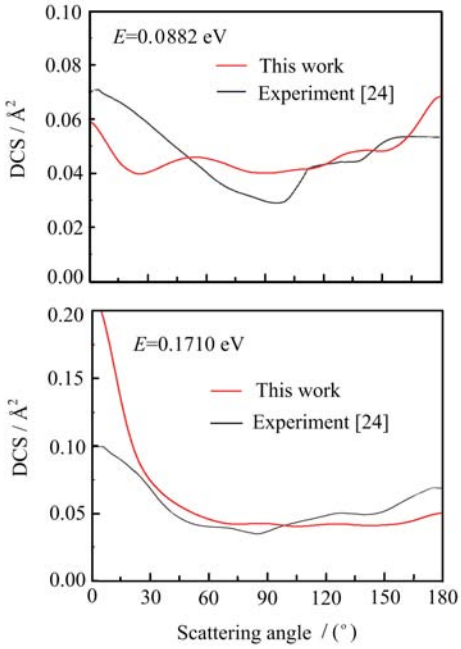


FIG. 8 The differential cross section of Li+HF reaction comparison with experiment data [24] at collision energy 0.0882 and 0.1710 eV.

### C. Isotope effects: the Li+DF reaction

In order to determine the isotopic effect and different initial rotation state effect on title reaction, the Li+DF($v$=0, $j$=0 and 1) reaction are investigated also in the present work. The initial rotational state effects on the Li+HF reaction have been investigated by Roncero and his co-workers [46].

The total reaction probabilities of Li+DF($v$=0, $j$=0) system for several total angular momentum $J$ are ploted in Fig.9. Comparing with the results in Fig.2, we can see that total reaction probabilities of the Li+DF reaction are apparently lower than those of the Li+HF reaction. As indicated by the results, there is a small threshold for the Li+DF reaction, whereas for the Li+HF system there is no threshold energy. These observations

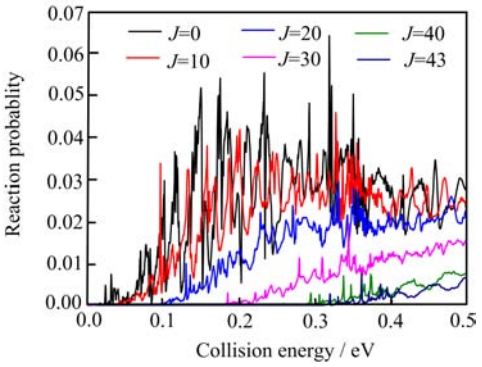


FIG. 9 Total reaction probabilities of the Li+DF($v$=0, $j$=0) reaction for several selected total angular momentum $J$ as a function of collision energy.

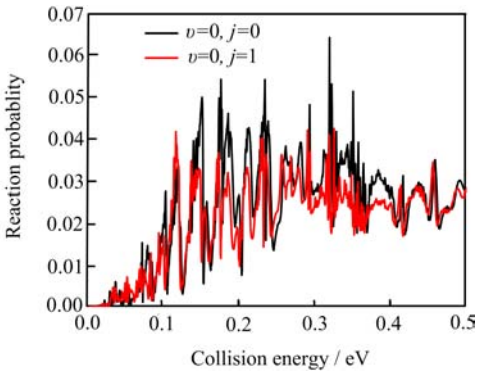


FIG. 10 Total reaction probabilities for the Li+DF($v$=0, $j$=0, 1)→ LiF+D reaction with the total angular momentum $J$=0.

are consistent with the previous theoretical work [38]. The fact that the reaction probabilities decrease when the H atom is substituted by the heavier isotopes originates from the difference in the zero point energies of HF and DF molecule and tunnelling effects. When the H atom is substituted by the D atom and forming DF molecule, the zero point energy becomes smaller thus the available total energy for the reaction decreases. At the same time, the quantum tunneling effect becomes much weaker. Unlike the reaction of Li+HF, the peaks arises from strong resonaces in the whole collision energy range 0−0.5 eV.

Total reaction probabilities of the Li+DF($v$=0, $j$=0, 1) reaction are plotted in Fig.10 for collision energy range from 0 eV to 0.5 eV. The initial rotational excitation of DF molecule have little effect on the reaction, in contrast with that of the Li+HF reaction [46]. The product rotational state-resolved reaction probabilities of the Li+DF reaction are plotted in Fig.11 for collision energy from 0 eV to 0.5 eV. It is observed that the reaction probabilities of even $j'$ are significantly higher than those of the odd $j'$ and such difference decrease with increasing $j'$, which is similar to that of the Li+HF reaction [46].

DOI:10.1063/1674-0068/28/cjcp1507151 ©2015 Chinese Physical Society

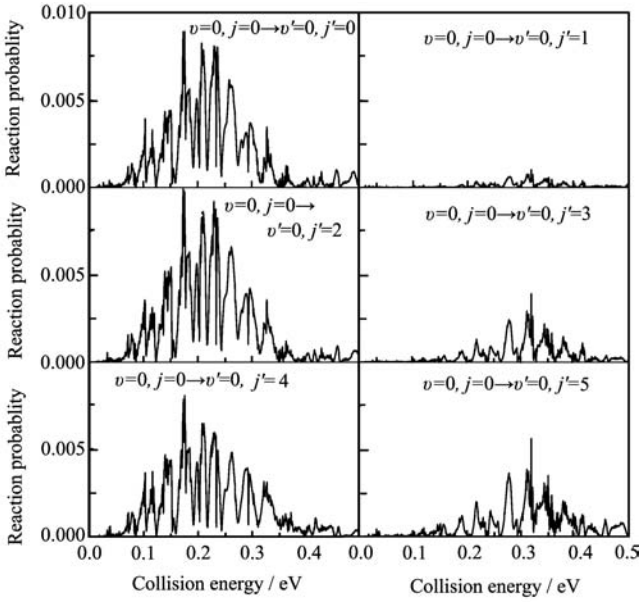


FIG. 11 Rotational state-resolved reaction probabilities for the Li+DF($v$=0, $j$=0)→LiF($v'$=0, $j'$=0−5)+D reaction with total angular momentum $J$=0. Significant difference in producing the rotational state of odd and even number appears.

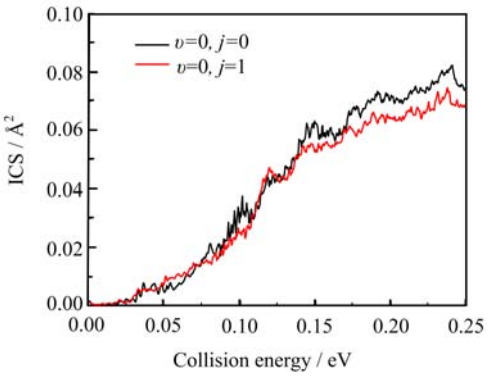


FIG. 12 Total integral cross section of the Li+DF($v$=0, $j$=0, 1)→LiF+D reaction.

The total ICS of the Li+DF reaction are plotted in Fig.12 for collision energy from 0 eV to 0.25 eV. The ICS of the Li+DF reaction simply increases with increasing collision energy, compared with that of the Li+HF reaction, due to the difference in the zero point energies and tunnelling effect. The ICSs for $j$=0 and $j$=1 of the Li+DF reaction are very similar, and both of them increase as the collision energy increases.

The product rotational state-resolved ICSs as a function of collision energy of the Li+DF($v$=0, $j$=0, 1) reaction are presented in Fig.13. Again, the results with initial rotational state $j$=0 and 1 are rather similar. All of the amplitude of ICSs increase with the increasing collision energy, reaching maximum at collision energy of 0.18 eV. The ICSs also increase with increasing quantum number of the rotational sate. At the same time, there are oscillations which suggests that the role of the resonances persist after summation of all partial waves.

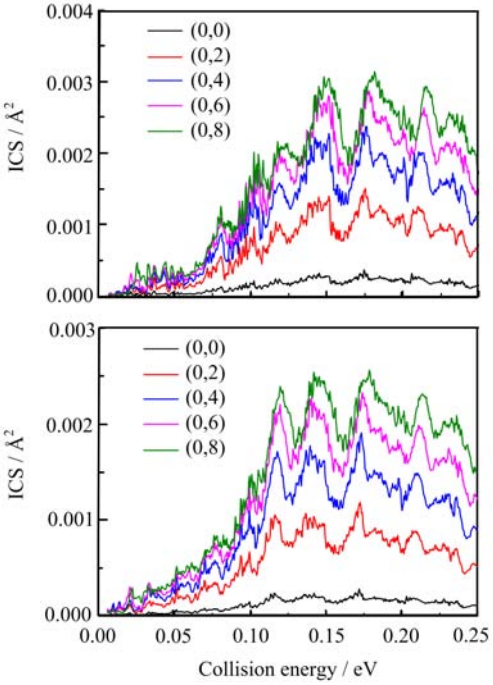


FIG. 13 Product rotational state-resolved ICSs of the Li+DF($v$=0, $j$=0 and 1) reaction. The upper panel is for initial state with $j$=0, and the lower panel is for $j$=1. The values in the bracket denote the quantum numbers of the product vibrational and rotational states.

The rotational state distributions for the Li+DF($v$=0, $j$=0, 1) reaction at four selected collision energies are presented in Fig.14. They are quite similar with initial rotational state of $j$=0 to $j$=1, and also similar to those for the Li+HF reaction with initial state of $j$=0. However, at relative lower collision energy, the rotational state distribution is hotter for the Li+DF reaction, and at relative higher collision energy, the rotational state distribution for the Li+HF reaction is hotter, especially for $v'$=0.

The DCSs of the Li+DF reaction with the initial state ($v$=0, $j$=0, 1) are presented in Fig.15 at the same collision energies of the Fig.7 in comparision with the Li+HF reaction. Essentially, the DCSs for these two isotope reaction are similar. At low collision energy, the DCS is nearly forward-backward symmetric and with increasing collision energy, becomes more and more forward-biased. However, in the studied collision energy range, there is more side scattering for the Li+DF reaction. Comparing the results in the left and right panel, it is observed that there is little difference for different initial rotational state $j$=0 and 1.

DOI:10.1063/1674-0068/28/cjcp1507151 ©2015 Chinese Physical Society

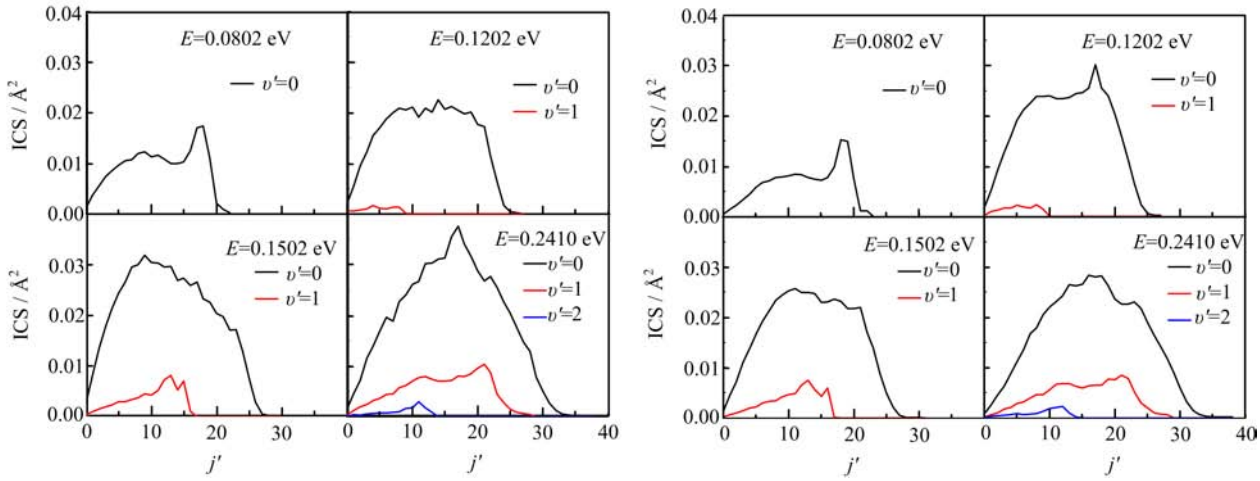


FIG. 14 Product rotational state distributions for the Li+DF($v$=0, $j$=0 , 1) reaction at four selected collision energies. The left panel is for initial state $j$=0 , and the right panel is for $j$=1.

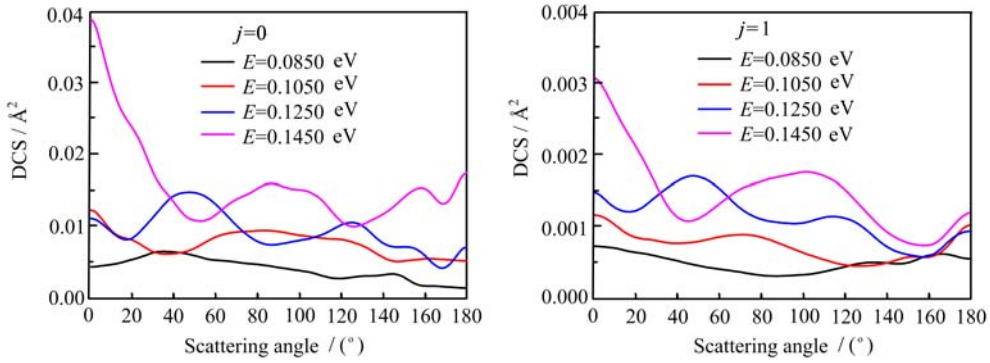


FIG. 15 The differential cross section of the Li+DF($v$=0, $j$=0, 1) reaction for some selected collision energies.

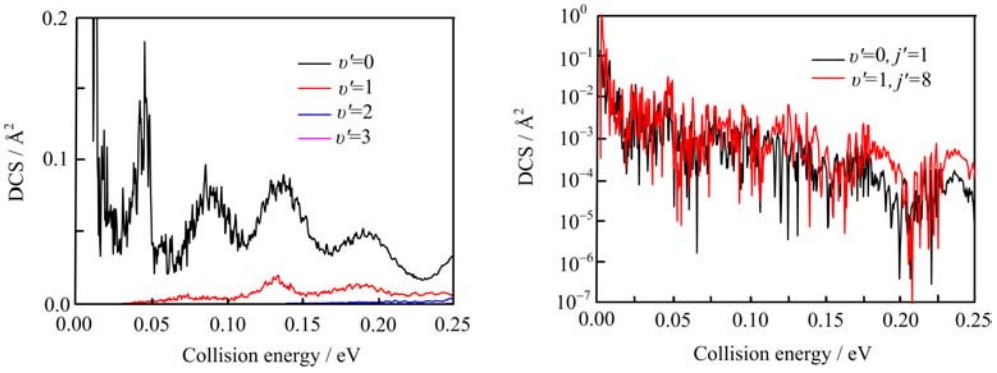


FIG. 16 The vibrational (left panel) and rotational (right panel) state-resolved backward scattering of the Li+HF reaction.

### D. Identification of the resonances in Li+DF/HF reaction

The resonance signatures often are smeared out after partial waves summation or by the overlap of a number of resonance states. Sometimes, they survive in the backward scattering [53, 54] or product ro-vibrational state-resolved ICS as oscillations, exhibiting as explicit signature of the existence of resonances. As observed from Fig.5 and Fig.13, the product rotational state-resolved ICSs do exhibit oscillations, especially the results in Fig.5 for the Li+HF reaction, which suggests that there are resonances possibly being identifiable. The product rotational state-resolved backward scatterings are superimposed by many sharp resonance peaks, which are difficult to capture with experiments of limited resolution, as shown in the left panel of Fig.16 and

DOI:10.1063/1674-0068/28/cjcp1507151 ©2015 Chinese Physical Society

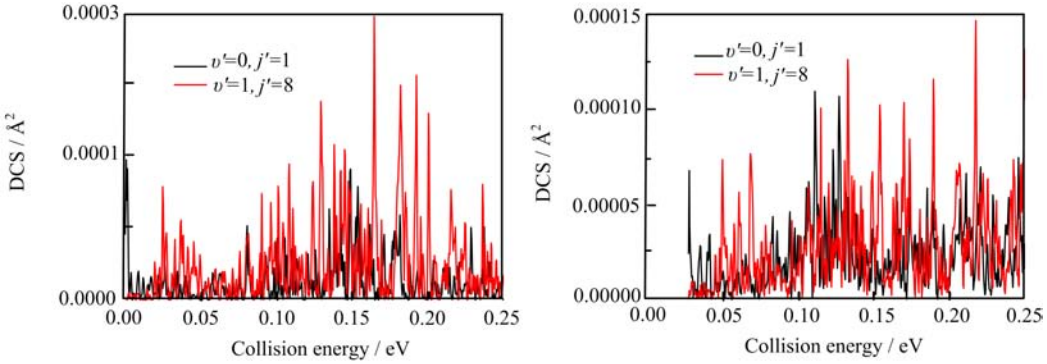


FIG. 17 The rotational resolved backward scattering of the Li+DF($v$=0, $j$=0 (left panel), 1 (right panel)) reaction.

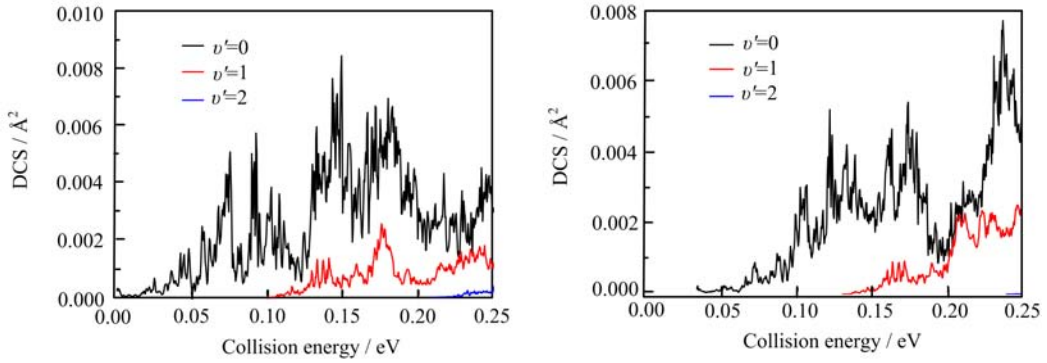


FIG. 18 The vibrational resolved backward scattering of the Li+DF($v$=0, $j$=0 (left panel), 1 (right panel)) reaction.

Fig.17. At the same time, there are also slow oscillations in the plots of right panel of Fig.16, which are essentially similar to those oscillations in Fig.5 and may be detectable by current molecular crossed beam.

The product vibrational state-resolved backward scattering (Fig.17) and ICSs of the Li+HF reaction (Fig.19) exhibit nice regular slow oscillations as a function of collision energy. These oscillations very possibly imply identifiable resonance states. This is unlike to the case of the Li+DF reaction (Fig.18 and Fig.20), whose product vibrational state-resolved ICSs and backward scattering exhibit many irregular sharp peaks. A clear relationship between the resonance states and the peaks is difficult to achieve.

The results in Fig.17, Fig.18, and Fig.20 suggest clearly again that there is little difference for the reaction Li+DF with reactant of initial rotational state $j$=0 and 1.

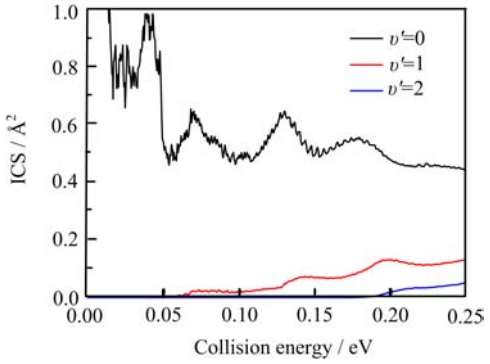


FIG. 19 The vibrational state-resolved integral cross section of the Li+HF($v$=0, $j$=0) reaction.

### E. Reaction rate constants

The initial state specific reaction rate constant of Li+HF($v$=0, $j$=0) and the values obtained by Ref.[49] using APW PES are presented in Fig.21 in the temperature range of 0−300 K. They are rather similar and decrease with increasing temperature. However, it is interesting to see that the larger value of our present total ICS but leads to lower reaction rate constant. The reason is unknown and might be due to the inaccuracy of the description of the reactivity at extremely low collision energy using wavepacket method. The initial state specific reaction rate constants of the Li+DF($v$=0, $j$=0, 1) reaction in the range of temperatures between 200 and 1000 K is presented in Fig.22. The rate con-

DOI:10.1063/1674-0068/28/cjcp1507151 ©2015 Chinese Physical Society

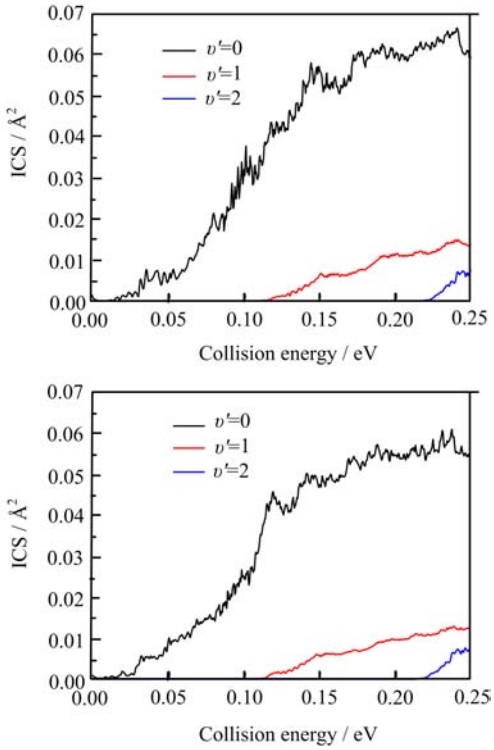


FIG. 20 The vibrational state-resolved integral cross section of the Li+DF($v$=0, $j$=0 (upper panel), 1 (lower panel)) reaction. The ICS of $v$=2 has been multiplied by a factor of 5.

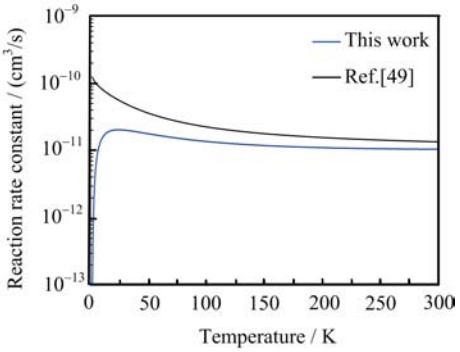


FIG. 21 Initial state specific rate constant of the Li+HF($v$=0, $j$=0) reaction.

stants for $j$=0 and $j$=1 are rather closed, as expected from their total ICS in Fig.12. The rate constant of the Li+HF($v$=0, $j$=0) reaction is not sensitive to the temperature and almost dose change in the temperature of 20−300 K. However, for the Li+DF($v$=0, $j$=0, 1) reaction, the thermal rate constants increase roughly by a factor of 10 in the temperature range considered. It is expected that the thermal reaction rate constant of Li+DF should be very similar to the results shown in Fig.22.

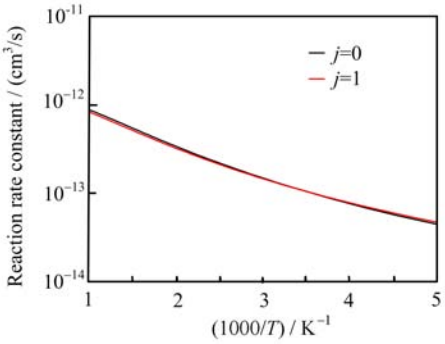


FIG. 22 Initial state specific reaction rate constant of the Li+DF($v$=0, $j$=0, 1) reaction.

## IV. CONCLUSION

The dynamics of the Li+HF reaction with initial state ($v$, $j$)=(0, 0) and the Li+DF reaction with initial state ($v$, $j$)=(0, 0) and (0, 1) were investigated by the time depended wave packet approach using the APW PES. The total reaction probabilities, the initial state specified reaction rate constant, ICSs and DCSs have been calculated. The total reaction probabilities for the Li+HF reaction were compared with the results reported by previous studies. There is much denser and sharper peaks around collision energy ∼0.05 eV for the Li+HF reaction than for the Li+DF reaction. The reactivity of the Li+HF reaction is much larger than the Li+DF reaction, due to more effective tunnelling effects of the H atom. The distribution of the product ro-vibrational states of these two reactions are rather similar, and the DCSs is backward-forward symmetric at low collision energy but becomes forward-biased with increasing collision energy. As compared with the Li+HF reaction, there is more side scattering for the Li+DF reaction. The rotational excitation of the reactant has little effect on the Li+DF reaction. For the Li+HF reaction, the thermal rate constant is not sensitive to the temperature and has a little negative temperature dependence. For the Li+DF reaction, the thermal rate constant increase roughly by a factor of 10 in the temperature range from 200 K to 1000 K. The signature of dense resonances are smeared out in the backward scattering for the Li+DF/HF reactions. However, milder oscillation survives in the product rotational and vibrational state-revolved ICSs of the reaction Li+DF($v$=0, $j$=0, 1) and product rotational and vibrational state-resolved backward scattering for of the reaction Li+HF, possibly due to a cluster of resonance states nearby which share some common features.

## V. ACKNOWLEDGMENTS

This work was supported by the National Basic Research Program of China (No.2013CB922200),

 ©2015 Chinese Physical Society

the National Natural Science Foundation of China (No.21222308, No.21103187, and No.21133006), the Chinese Academy of Sciences, and the Key Research Program of Chinese Academy of Sciences.

[1] E. H. Taylor and A. Datz, J. Chem. Phys. **23**, 1711 (1955).
[2] D. R. Herschbach, Adv. Chem. Phys. **10**, 319 (1966).
[3] Y. Zeiri and M. Shapiro, Chem. Phys. **31**, 217 (1978).
[4] M. M. L. Chen and H. F. Schaefer, J. Chem. Phys. **72**, 4376 (1980).
[5] S. Carter and J. N. Murrell, Mol. Phys. **41**, 567 (1980).
[6] M. Garcia and A. Laganà, Mol. Phys. **52**, 1115 (1984).
[7] M. Paniagua and A. Aguado, Chem. Phys. **31**, 287 (1989).
[8] A. Aguado, C. Suárez, and M. Paniagua, Chem. Phys. **201**, 107 (1995).
[9] A. Laganà, O. Gervasi, and E. Garcia, Chem. Phys. Lett. **143**, 174 (1988).
[10] A. Laganà, O. G. Aspuru, and E. Garcia, J. Chem. Phys. **108**, 3886 (1998).
[11] C. Suárez, A. Aguado, C. Tablero, and M. Paniagua, Int. J. Quantum Chem. **52**, 935 (1994).
[12] R. Burcl, P. Piecuch, V. Špiko, and O. Bludský, Int. J. Quantum Chem. **80**, 916 (2000).
[13] A. Aguado, M. Paniagua, M. Lara, and O. Roncero, J. Chem. Phys. **106**, 1013 (1997).
[14] A. Aguado, M. Paniagua, M. Lara, and O. Roncero, J. Chem. Phys. **107**, 10085 (1997).
[15] A. W. Jasper, M. D. Hack, A. Chakraborty, D. G. Truhlar, and P. Piecuch, J. Chem. Phys. **115**, 7945 (2001).
[16] A. W. Jasper, M. D. Hack, D. G. Truhlar, and P. Piecuch, J. Chem. Phys. **116**, 8353 (2002).
[17] A. Aguado, M. Paniagua, C. Sanz, and O. Roncero, J. Chem. Phys. **119**, 10088 (2003).
[18] A. Aguado, M. Paniagua, and H. J. Werner, http://www.theochem.uni-stuttgart.de/werner/lihf/potential/APW*pes*_LiHF.f. (2004).
[19] C. H. Becker, P. Casavecchia, P. W. Tiedemann, and J. J. Valentini, J. Chem. Phys. **73**, 2833 (1980).
[20] H. J. Loesch and F. Stienkemeier, J. Chem. Phys. **98**, 9570 (1993).
[21] H. J. Loesch and F. Stienkemeier, J. Chem. Phys. **99**, 9598 (1993).
[22] F. J. Aoiz, E. Verdasco, V. S. Rábanos, H. J. Loesch, M. Menéndez, and F. Stienkemeier, Phys. Chem. Chem. Phys. **2**, 541 (2000).
[23] O. Höbel, M. Menéndez, and H. J. Loesch, Phys. Chem. Chem. Phys. **3**, 3633 (2001).
[24] O. Höbel, R. Bobbenkamp, A. Paladini, A. Russo, and H. J. Loesch, Phys. Chem. Chem. Phys. **6**, 2198 (2004).
[25] R. Bobbenkamp, A. Paladini, A. Russo, H. J. Loesch, and M. Menéndez, J. Chem. Phys. **122**, 244304 (2005).
[26] J. M. Alvariño, P. Casavecchia, O. Gervasi, and A. Laganà, J. Chem. Phys. **77**, 6341 (1982).
[27] D. L. Miller and R. E. Wyatt, J. Chem. Phys. **86**, 5557 (1987).
[28] H. J. Loesch,E. Stenzel, and B. Wüstenbecker, J. Chem. Phys. **95**, 3841 (1991).
[29] G. G. BalintKurti, F. Gögtas, S. P. Mort, A. R. Offer, and A. Laganà, J. Chem. Phys. **99**, 9567 (1993).
[30] M. Baer, I. Last, and H. J. Loesch, J. Chem. Phys. **101**, 9648 (1994).
[31] G. A. Parker, A. Laganà, S. Crocchianti, and R. T. Pack, J. Chem. Phys. **102**, 1238 (1995).
[32] F. Gögtas, G. G. BalintKurti, and A. R. Offer, J. Chem. Phys. **104**, 7927 (1996).
[33] J. M. Alvariño, V. Aquilanti, S. Cavalli, S. Crocchianti, and A. Laganà, J. Chem. Phys. **107**, 3339 (1997).
[34] M. Lara, A. Aguado, O. Roncero, and M. Paniagua, J. Chem. Phys. **109**, 9391 (1998).
[35] J. M. Alvariño, V. Aquilanti, S. Cavalli, S. Crocchianti, A. Laganà, and T. Martinez, J. Phys. Chem. A **102**, 9638 (1998).
[36] F. J. Aoiz, M. T. Martínez, M. Menéndez, V. S. Rábanos, and E. Verdasco, Chem. Phys. Lett. **299**, 25 (1999).
[37] M. Lara, A. Aguado, M. Paniagua, and O. Roncero, J. Chem. Phys. **113**, 1781 (2000).
[38] A. Laganà, A. Bolloni, and S. Crocchianti, Phys. Chem. Chem. Phys. **2**, 535 (2000).
[39] F. J. Aoiz, M. T. Martínez, and V. S. Rábanos, J. Chem. Phys. **114**, 8880 (2001).
[40] D. Xie, S. Li, and H. Guo, J. Chem. Phys. **116**, 6391 (2002).
[41] P. F. Weck and N. Balakrishnan, J. Chem. Phys. **122**, 154309 (2005).
[42] P. F. Weck and N. Balakrishnan, J. Chem. Phys. **122**, 234310 (2005).
[43] D. Skouteris, S. Crocchianti, and A. Laganà, Chem. Phys. Lett. **440**, 1 (2007).
[44] D. Skouteris, S. Crocchianti, and A. Laganà, Chem. Phys. **349**, 170 (2008).
[45] A. Zanchet, O. Roncero, T. González-Lezana, A. Rodríguez-López, A. Aguado, C. Sanz-Sanz, and S. Gómez-Carrasco, J. Phys. Chem. A **113**, 14488 (2009).
[46] L. González-Sánchez, O. Vasyutinskii, A. Zanchet, C. Sanz-Sanz, and O. Roncero, Phys. Chem. Chem. Phys. **13**, 13656 (2011).
[47] Z. Sun, H. Guo, and D. H. Zhang, J. Chem. Phys. **132**, 084112 (2010).
[48] Z. Sun, S. Lee, H. Guo, and D. H. Zhang, J. Chem. Phys. **130**, 174102 (2009).
[49] J. Hazra and N. Balakrishnan, New. J. Phys. **17**, 055027 (2015).
[50] R. Bobbenkamp, H. Loesch, M. Mudrich, and F. Stienkemeier J. Chem. Phys. **135**, 204306 (2011).
[51] Z. Sun, W. T. Yang, and D. H. Zhang, Phys. Chem. Chem. Phys. **14**, 1827 (2012).
[52] W. T. Li, D. H. Zhang, and Z. Sun, J. Phys. Chem. A **118**, 9801 (2014).
[53] T. Wang, J. Chen, T. G. Yang, C. L. Xiao, Z. Sun, L. Huang, D. X. Dai, X. M. Yang, and D. H. Zhang Science **342**, 1499 (2013).
[54] T. G. Yang, J. Chen, L. Huang, T. Wang, C. L. Xiao, Z. Sun, D. X. Dai, X. M. Yang, and D. H. Zhang, Science **347**, 60 (2015).

DOI:10.1063/1674-0068/28/cjcp1507151 ©2015 Chinese Physical Society